J|A|C|S
ARTICLES
Published on Web 12/18/2003

Insights into the Phosphoryl-Transfer Mechanism of cAMP-Dependent Protein Kinase from Quantum Chemical Calculations and Molecular Dynamics Simulations

Natalia Díaz and Martin J. Field*

Contribution from the Laboratoire de Dynamique Moléculaire, Institut de Biologie Structurale - Jean-Pierre Ebel, CEA/CNRS, 41, rue Jules Horowitz, F-38027 Grenoble Cedex 1, France

Received July 15, 2003; E-mail: mjfield@ibs.fr

Abstract: To investigate the molecular details of the phosphoryl-transfer mechanism catalyzed by cAMP-dependent protein kinase, we performed quantum mechanical (QM) calculations on a cluster model of the active site and molecular dynamics (MD) simulations of a ternary complex of the protein with Mg_2ATP and a 20-residue peptide substrate. Overall, our theoretical results confirm the participation of the conserved aspartic acid, Asp_{166}, as an acid/base catalyst in the reaction mechanism catalyzed by protein kinases. The MD simulation shows that the contact between the nucleophilic serine side chain and the carboxylate group of Asp_{166} is short and dynamically stable, whereas the QM study indicates that an Asp_{166}-assisted pathway is structurally and energetically feasible and is in agreement with previous experimental results.

Introduction

The reversible phosphorylation of proteins regulates almost all aspects of cell life, ranging from metabolic pathways to cell cycle control and gene transcription.[1] In addition, abnormal phosphorylation turns out to be a cause or consequence of several diseases, and many naturally occurring toxins and pathogens exert their effects by altering the phosphorylation state of proteins.[2] As a result, the enzymes that control this process, protein kinases and phosphatases, have become important targets for rational drug design.

Protein kinases catalyze the transfer of the γ-phosphoryl group of ATP to the hydroxyl side chain of specific serine, threonine or tyrosine residues in their target proteins with the assistance of Mg^{2+} ions. The protein kinase family of enzymes is large and structurally diverse although all the members are characterized by a conserved catalytic core with a bilobal structure,[3−5] which suggests a shared catalytic mechanism. The small *N*-terminal lobe is dominated by a five stranded antiparallel β-sheet and a long α-helix. The first two strands of the β-sheet and the turn connecting them form the characteristic glycine-rich sequence which covers the whole ATP molecule in the active site, whereas the third β-strand contains an invariant lysine residue that interacts with the phosphate groups of ATP (see Figure 1). The larger C-terminal lobe, which contributes significantly to substrate binding, is mostly helical. Two essential structural elements of this large lobe are the activation segment, in which the phosphorylation state of an Ser/Thr residue usually regulates the activity of the enzyme, and the catalytic loop, which includes a conserved aspartic acid proposed to act as a base catalyst during the phosphoryl-transfer reaction. The active site is located at the interface between the small and large lobes forming a deep cleft. The nucleoside moiety of ATP is completely buried in this cleft, whereas the triphosphate arm, the Mg^{2+} ions, and the peptide/protein substrate are located at the mouth of the opening where the phosphoryl-transfer reaction takes place (see Figure 1).

The cAMP-dependent protein kinase (or Protein Kinase A, PKA) is the best characterized member of this large family of enzymes, physiologically, biochemically, and structurally. It recognizes many physiological substrates and controls a diversity of cellular processes.[6] The inactive PKA holoenzyme is a tetramer composed of two regulatory and two catalytic subunits that become dissociated after the second messenger cAMP (cyclic-adenosine monophosphate) binds to the regulatory subunits. As a result, the catalytically competent form of PKA (C-subunit) is composed of only one domain of about 350 amino acids, which is often considered a prototype for the catalytic core of the whole kinase family.[7]

The catalytic cycle of the C-subunit of PKA was studied by a number of techniques. Both steady-state kinetic and isotope partitioning experiments demonstrated that PKA binds ATP and peptide substrates randomly, although initial binding of ATP is preferred.[10] In contrast, product release is ordered with phosphopeptide leaving the active site first.[11]

PKA requires the assistance of an essential high affinity Mg^{2+} ion that is coordinated by the β and γ phosphates of ATP, the

(1) Johnson, L. N.; Nobel, M. E. M.; Owen, J. *Cell* **1996**, *85*, 149−158.
(2) Cohen, P. *Eur. J. Biochem.* **2001**, *268*, 5001−5010.
(3) Hanks, S. K.; Quinn, A. M.; Hunter, T. *Science* **1988**, *241*, 42−52.
(4) Taylor, S. S.; Radzio-Andzelm, E. *Structure* **1994**, 345−355.
(5) Bossemeyer, D. *FEBS Lett.* **1995**, *369*, 57−61.
(6) Shabb, J. B. *Chem. Rev.* **2001**, *101*, 2381−2411.
(7) Johnson, D. A.; Akamine, P.; Radzio-Andzelm, E.; Madhusudan; Taylor, S. S. *Chem. Rev.* **2001**, *101*, 2243−2270.
(8) Kraulis, P. J. *J. Appl. Crystallogr.* **1991**, *24*, 946−950.
(9) Merritt, E. A.; Bacon, D. J. *Methods Enzymol.* **1997**, *277*, 505−524.
(10) Kong, C. T.; Cook, P. F. *Biochemistry* **1988**, *27*, 4795−4799.
(11) Shaffer, J.; Adams, J. A. *Biochemistry* **1999**, *38*, 12072−12079.

Figure 1. Ribbon representation of the catalytic subunit of PKA (in blue) in a ternary complex with Mg_2ATP (ball-and-stick) and a 20-residue peptide substrate (in red) resulting from the initial MM geometry optimization. The small and large lobes and the N- and C-terminal segments are identified with different gradations of blue. Lys_{72} in β-strand 3 of the small lobe, Asp_{166} in the catalytic loop, and the phosphorylated Thr_{197} in the activation loop of the large lobe, as well as the P-site serine of the substrate, are represented as sticks. Figure produced with Molscript[8] and Raster3D.[9]

Scheme 1

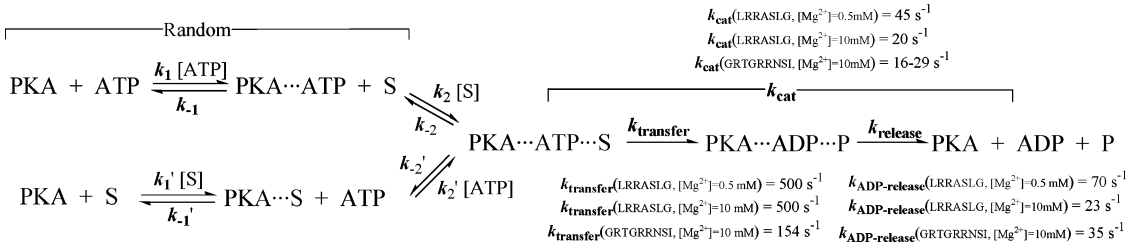

side chain of the invariant residue Asp_{184}, and two water molecules. In addition, at high magnesium concentrations, a second low affinity site becomes coordinated by the α and γ phosphates of ATP, the side chains of Asn_{171} and Asp_{184}, and one water molecule. Kinetic analyses performed with PKA and a peptide model substrate (LRRASLG, kemptide) at various metal ion concentrations have shown that an increase in magnesium ion concentration from 0.5 mM to 10.0 mM results in a decrease of the rate for turnover from 45 s^{-1} to 20 s^{-1} (see k_{cat} in Scheme 1).[12] As a consequence, the secondary metal binding site is usually termed the *inhibitory* site. However, the inhibitory effect on k_{cat} of the second metal ion is offset by a lower K_{ATP} so that k_{cat}/K_{ATP} actually increases with the metal ion concentration. In this sense, the term *inhibitory* metal is somewhat misleading as has been remarked by some authors.[13] On the other hand, the effects of solvent viscosity on the steady-state kinetic parameters suggest that maximum turnover is completely limited by ADP dissociation at high magnesium concentrations ($k_{release} \approx 23$ s^{-1} in Scheme 1).[14] At low magnesium concentrations, the net rate constant for product release ($k_{release} \approx 70$ s^{-1}) controls k_{cat} only partially since catalytic trapping studies showed that a conformational change with a rate constant of 170 s^{-1} also limits turnover.[11] While this conformational step may still occur under high magnesium concentrations, the increased affinity for ADP in these conditions determines that only ADP release limits turnover.[11]

In contrast with the product release step of the PKA catalyzed reaction, rapid quench flow techniques have demonstrated that the rate of the chemical step (the transfer of the γ-phosphoryl group from ATP to the substrate) is similar at both 0.5 mM and 10 mM concentrations of free Mg^{2+}, even though the occupation of the second metal binding site varies from 20% to 80%. The chemical step is characterized by a remarkable rate constant of 500 s^{-1} for the phosphorylation of kemptide (see Scheme 1). The magnitude of this rate constant seems to vary with the nature of the peptide substrate. Thus the rate constant for the phosphorylation of the peptide model GRTGRRNSI is 154 s^{-1}, whereas the dissociation rate constant for ADP is 35 s^{-1} and partially limits turnover ($k_{cat} = 16-29$ s^{-1} in Scheme 1).[15,16]

Despite the extensive structural and kinetic characterization of the cAMP-dependent protein kinase, the detailed chemical

(12) Shaffer, J.; Adams, J. A. *Biochemistry* **1999**, *38*, 5572−5581.
(13) Adams, J. A. *Chem. Rev.* **2001**, *101*, 2271−2290.
(14) Adams, J. A.; Taylor, S. S. *Biochemistry* **1992**, *31*, 8516−8522.

mechanism for the phosphoryl-transfer step remains elusive. According to stereochemical analyses performed at high magnesium concentrations, the phosphoryl-transfer reaction proceeds with inversion of configuration at the γ-phosphoryl group, which is consistent with a direct in-line nucleophilic displacement.[17] The pH dependence of the apparent second-order rate constant $k_{cat}/K_{kemptide}$ for kemptide phosphorylation is bell-shaped with limiting pK_a values of approximately 6.2 and 8.5.[18] Initially, the lowest pK_a value was attributed to a hypothetical base catalyst that would activate the nucleophilic hydroxyl group during the phosphoryl-transfer reaction. This hypothesis was supported by the X-ray structure of PKA complexed with ADP and a peptide substrate in which the hydroxyl group of the nucleophilic serine and the strictly conserved Asp_{166} establish a hydrogen-bond (H-bond) interaction.[19] Moreover, mutagenesis experiments performed at high magnesium concentrations showed a 370-fold reduction in the k_{cat} of the Asp166Ala mutant enzyme.[20] However, according to kinetic analyses performed with PKA and four peptide substrates, the lowest pK_a value corresponds to the ionization of an enzyme residue interacting with the P-2 arginine of the peptide substrate,[21] not to deprotonation of the invariant Asp_{166}. Therefore, the pK_a of Asp_{166} seems to be lower than 6, and so it is not basic enough to accept a proton from the serine side chain in the ground state. Alternatively, to explain the catalytic impact of Asp_{166} observed in the mutagenesis experiments, it has been proposed that this residue helps position the nucleophilic hydroxyl group for productive displacement toward the γ-phosphoryl of ATP through the H-bond contact observed in the crystallographic structure.[15]

The catalytic subunit of PKA without substrates in the active site has been studied using molecular dynamics (MD) simulations and the AMBER force field.[22] Previous theoretical work has also studied the reaction mechanism catalyzed by PKA by means of semiempirical quantum mechanics (QM) and hybrid quantum mechanics/molecular mechanics (QM/MM) methodologies.[23,24] The selected model systems contained two magnesium ions in the kinase active site, and it was proposed that the energetically favored mechanism is one in which the nucleophilic substitution takes place with direct proton transfer to an O atom of the γ-phosphoryl group of ATP, rather than one in which Asp_{166} accepts the proton from the nucleophilic hydroxyl group. It must be noted, however, that ab initio and density functional theory (DFT) QM/MM calculations have shown that semiempirical methods are inadequate to properly describe the active site of protein kinases,[25] so that mechanistic conclusions obtained from previous semiempirical calculations require confirmation. The most recent theoretical studies of the PKA reaction mechanism have employed DFT methods to investigate various cluster models of the active site. In one study, Hirano et al. predicted a high energy barrier of 36 kcal/mol although they neglected the catalytic effect of Asp_{166}.[26] In a second study, that appeared after our paper was submitted, Valiev et al. characterized a reaction pathway with direct participation of the carboxylate group of Asp_{166}, resulting in a phosphorylated serine side chain in interaction with a protonated Asp_{166}.[27] In this case, the reported energy barrier (11 kcal/mol) was in reasonable agreement with the measured kinetic constant. However, it must be noted that a comparative analysis of different mechanisms (with and without the assistance of Asp_{166}) using the same active-site model and the same level of theory has not been presented in previous DFT studies.

In this work we characterized the chemical mechanism catalyzed by PKA by performing a molecular dynamics (MD) simulation of the ternary PKA···Mg_2ATP···Peptide complex and DFT geometry optimizations of a large cluster model of the enzyme's active site. The MD simulations enabled us to determine the dynamical stability and strength of the most important noncovalent contacts: kinase−ATP, kinase−substrate, and ATP−substrate, whereas the DFT calculations allowed us to characterize two different reaction mechanisms for the phosphoryl-transfer reaction that differ in the role played by the carboxylate side chain of the invariant Asp_{166} along the reaction coordinate. Together the presence of long-lived specific prereactive contacts during the MD simulation and the energetic data obtained from the QM calculations on the cluster model give new insight into the phosphoryl-transfer mechanism catalyzed by protein kinases.

Methods

Setup of the System. Starting coordinates were taken from the crystallographic structure of the cAMP-dependent protein kinase catalytic subunit at a 2.0 Å resolution (PDB ID code: 1CDK).[28] This structure is a ternary complex with an ATP analogue (AMP-PNP), two Mn^{2+} ions, and the 20-residue peptide inhibitor PKI(5−24) located in the kinase active site. To build up our model of the enzyme−substrates system, we manually transformed AMP-PNP and the two Mn^{2+} ions into ATP and two Mg^{2+} ions, respectively. In addition, the P-site alanine of the peptide inhibitor was mutated into a nucleophilic serine residue giving the 20-residue peptide substrate with the sequence TTYADFIASGRTGRRNSIHD. In agreement with the initial X-ray structure and with previous theoretical work, we decided to place two Mg^{2+} ions in the PKA active site. It is to be noted that all the crystal structures of ternary complexes of PKA have both metal binding sites occupied and that mutagenesis experiments, performed to highlight the catalytic relevance of the Asp_{166} residue, were done at high magnesium concentrations. Kinetic measurements have also shown that the rate constant for the chemical step is the same at high and low magnesium concentrations.[12] Finally, PKA is usually considered a prototype for the catalytic core of the whole protein kinase family, and the requirement of two magnesium ions for catalytic activity is well established for some of these other enzymes.[13,29]

The protonation state for titrable amino acids of the kinase and peptide substrate was assigned according to pK_a calculations performed with the UHBD program.[30] We employed the cluster method[31] with

(15) Zhou, J.; Adams, J. A. *Biochemistry* **1997**, *36*, 2977−2984.
(16) Zhou, J.; Adams, J. A. *Biochemistry* **1997**, *36*, 15733−15738.
(17) Ho, M.-F.; Bramson, H. N.; Hansen, D. E.; Knowles, J. R.; Kaiser, E. T. *J. Am. Chem. Soc.* **1988**, *110*, 2680−2681.
(18) Yoon, M.-Y.; Cook, P. F. *Biochemistry* **1987**, *26*, 4118−4125.
(19) Madhusudan; Trafny, E. A.; Xuong, N.; Adams, J. A.; Ten Eyck, L. F.; Taylor, S. S.; Sowadski, J. M. *Protein Sci.* **1994**, *3*, 176−187.
(20) Gibbs, C. S.; Zoller, M. J. *J. Biol. Chem.* **1991**, *266*, 8923−8931.
(21) Adams, J. A.; Taylor, S. S. *J. Biol. Chem.* **1993**, *268*, 7747−7752.
(22) Tsigelny, I.; Greenberg, J. P.; Cox, S.; Nichols, W. L.; Taylor, S. S.; Ten Eyck, L. F. *Biopolymers* **1999**, *50*, 513−524.
(23) Hart, J. C.; Sheppard, D. W.; Hillier, I. H.; Burton, N. A. *Chem. Commun.* **1999**, 79−80.
(24) Hutter, M. C.; Helms, V. *Protein Sci.* **1999**, *8*, 2728−2733.
(25) Sheppard, D. W.; A., B.; Hillier, I. H. *THEOCHEM* **2000**, *506*, 35−44.
(26) Hirano, Y.; Hata, M.; Hoshino, T.; Tsuda, M. *J. Phys. Chem. B* **2002**, *106*, 5788−5792.
(27) Valiev, M.; Kawai, R.; Adams, J. A.; Weare, J. H. *J. Am. Chem. Soc.* **2003**, *125*, 9926−9927.
(28) Bossemeyer, D.; Engh, R. A.; Kinzel, V.; Ponstingl, H.; Huber, R. *EMBO J.* **1993**, *12*, 849−859.
(29) Sun, G.; Budde, R. J. A. *Biochemistry* **1997**, *36*, 2139−2146.
(30) Antosiewicz, J.; McCammon, J. A.; Gilson, M. K. *J. Mol. Biol.* **1994**, *238*, 415−436.
(31) Gilson, M. K. *Proteins* **1993**, *15*, 266−282.

focusing grids on each of the titrable residues. Focusing was done in four steps with consecutive grid spacings of 5.0, 1.0, 0.5, and 0.25 Å. A dielectric constant of 80.0 was selected for the solvent. For the protein, we employed dielectric constants of 80.0, 40.0, 20.0, 15.0, 8.0, or 4.0 in order to check the dependence of the predicted pK_a value on the protein dielectric constant, and the values corresponding to $\epsilon_{protein} = 20.0$ were employed in the assignment of the protonation state. As a result, all ionizable residues (including Asp_{166}) were set to their normal ionization state at pH 7 with the exception of His_{87}, which was modeled in its protonated form. The predicted pK_a values for this residue range from 7.0 with $\epsilon_{protein} = 80.0$ to 12.2 with $\epsilon_{protein} = 4.0$, with an intermediate value of 8.20 for $\epsilon_{protein} = 20.0$. In addition, the initial crystal structure shows clear contacts between the Nϵ atom of His_{87} and one of the oxygen atoms of the phosphorylated threonine (Thr_{197}) located in the activation loop (2.7 Å) and between the Nδ atom and the Gln_{84} carbonyl side chain (2.7 Å). Other histidine residues of the protein and peptide substrate were modeled in a neutral state. The Nδ or Nϵ atoms were protonated according to electrostatic potential and pK_a calculations. Thus, His_{68}, His_{142}, His_{158}, and His_{260} were protonated at Nδ, whereas His_{39}, His_{62}, His_{131}, and His_{294} were protonated at Nϵ. The histidine present in the P + 2 position of the peptide substrate was protonated at its Nϵ atom.

Hydrogen atoms were added to the crystallographic heavy atoms using the HBUILD module[32] implemented in the CHARMM program.[33] Subsequently, the system was immersed in a box of TIP3P water molecules[34] that extended approximately 10 Å from the protein and substrate atoms. The solvent box was generated with CHARMM and equilibrated with molecular dynamics simulations. Upon insertion of the kinase ternary complex, along with its crystallographic water molecules, all solvent molecules overlapping crystallographic atoms were removed. In addition, 3 Cl^- counterions were manually placed in the box to neutralize the system. This resulted in an enzyme−substrates system (5995 atoms) solvated by the 163 X-ray water molecules and 11 044 additional solvent molecules.

MD Simulation. The all-atom CHARMM force field[35] (version 22) as implemented in the CHARMM program[33] (version 27b1) was used to represent the system during the MD simulation. To remove bad contacts in the initial X-ray solvated structure, ABNR (Adopted Basis Newton−Raphson) energy minimizations were done. Harmonic constraints were imposed on the position of the protein and substrate atoms during the minimization, but these were successively lowered and finally removed. After minimization, the system was heated from 0 to 300 K by means of 10 ps of Langevin dynamics employing a friction coefficient of 50 ps^{-1}.[36] Subsequently, we started a constant pressure and constant temperature (CPT) MD simulation[37] using the extended system pressure algorithm[38,39] and a Hoover thermostat to control the pressure (1 atm) and the temperature (300 K) of the system.[40,41] The time step was chosen to be 1.0 fs, and the SHAKE algorithm[42] was used to constrain all bonds involving water-molecule hydrogen atoms. A nonbond pairlist cutoff of 13.5 Å was used, and the nonbonded pairlist was updated every 20 time steps. Periodic boundary conditions were applied to simulate a continuous system. To include the contributions of long-range electrostatic interactions, the Particle-Mesh-Ewald (PME) method[43] was used with a grid spacing of ~1 Å and a fifth-order B-spline interpolation to compute the potential and forces between grid points. For van der Waals interactions, a shifting function was used between 8 and 12 Å.

An equilibration period of 300 ps resulted in a stable trajectory as indicated by the evolution of the energy components of the system and the root-mean-squared coordinate deviation (RMSD) of the protein core with respect to the initial X-ray structure. Subsequently, a 1.5 ns trajectory was computed, and coordinates were saved for analysis every 100 time steps. All of the MD results were analyzed using the ptraj module of the AMBER 7.0 suite of programs.[44]

QM Calculations. To calibrate the methodology used in the QM study of the enzymatic mechanism catalyzed by PKA, proton affinities for acetate and a methyl phosphate dianion interacting with zero, one, and two Mg^{2+} ions were evaluated at different levels of theory: AM1, PM3, B3LYP/6-31G*, B3LYP/6-31+G**//B3LYP/6-31G*, B3LYP/6-31+G**, MP2/6-31G*, and G2(MP2,SVP).[45−49] In addition, the same levels of theory were employed to locate a prereactive complex and a transition structure (TS) for the hydrolysis of the methyl phosphate dianion. All the structures included in the test set were further characterized by analytical computation of harmonic frequencies at the B3LYP/6-31G* level. Relative enthalpies were computed using the B3LYP/6-31G* frequencies within the ideal gas, rigid rotor, and harmonic oscillator approximations (298.15 K, 1 bar).[50] We employed the Jaguar4.2[51] program for the DFT calculations, the Gaussian98 suite of programs[52] for the MP2 and G2(MP2,SVP) calculations, and the DYNAMO library[53,54] for the semiempirical methods.

The enzymatic phosphoryl-transfer process was examined computationally by considering a cluster model of the PKA active site. Our cluster model included the side chains of Asp_{166}, Lys_{168}, Asn_{171}, and Asp_{184}, the methyltriphosphate arm of ATP, two Mg^{2+} ions, and the three water molecules which coordinate the metal ions in the X-ray structure. The side chain of the invariant Lys_{72} was modeled as a methylamonium group, resulting in a neutral model of the kinase active site (see Scheme 2). The initial coordinates for the cluster atoms were extracted from the previously edited 1CDK crystal structure after partial minimization of all protein and substrate atoms immersed in a layer of

(32) Brünger, A. T.; Karplus, M. *Proteins: Struct., Funct., Genet.* **1988**, *4*, 148−156.
(33) Brooks, B.; Bruccoleri, R. E.; Olafson, B. D.; States, D. J.; Swaminathan, S.; Karplus, M. *J. Comput. Chem.* **1983**, *4*, 187−217.
(34) Jorgensen, W. L.; Chandrasekhar, J.; Madura, J.; Impley, R. W.; Klein, M. L. *J. Phys. Chem.* **1983**, *79*, 926−935.
(35) MacKerell, A. D., Jr.; Bashford, D.; Bellott, M. et. al. *J. Phys. Chem. B* **1998**, *102*, 3586−3616.
(36) Feller, S. E.; Zhang, Y.; Pastor, R. W.; Brooks, B. R. *J. Chem. Phys.* **1995**, *103*, 4613−4621.
(37) Andersen, H. C. *J. Chem. Phys.* **1980**, *72*, 2384−2393.
(38) Martyna, G. J.; Klein, M. L.; Tuckerman, M. E. *J. Chem. Phys.* **1992**, *97*, 2635−2643.
(39) Martyna, G. J.; Tobias, D. J.; Klein, M. L. *J. Chem. Phys.* **1994**, *101*, 4177−4189.
(40) Nosé, S.; Klein, M. L. *Mol. Phys.* **1983**, *50*, 1055−1076.
(41) Nosé, S. *J. Chem. Phys.* **1984**, *81*, 511−519.
(42) van Gunsteren, W. F.; Berendsen, H. J. C. *Mol. Phys.* **1977**, *34*, 1311.
(43) Essman, V.; Perera, L.; Berkowitz, M. L.; Darden, T.; Lee, H.; Pedersen, L. G. *J. Chem. Phys.* **1995**, *103*, 8577−8593.
(44) Case, D. A.; Pearlman, D. A.; Caldwell, J. W.; Cheatham, T. E. I.; Wang, J.; Ross, W. S.; Simmerling, C. L.; Darden, T. A.; Merz, K. M.; Stanton, R. V.; Cheng, A. L.; Vincent, J. J.; Crow-Ley, M.; Tsui, V.; Gohlke, H.; Radmer, R. J.; Duan, Y.; Pitera, J.; Massova, I.; Seibel, G. L.; Singh, U. C.; Weiner, P. K.; Kollman, P. A. *AMBER*, 7.0 ed.: University of California: San Francisco, CA, 2002.
(45) Hehre, W. J.; Radom, L.; Schleyer, P. v. R.; Pople, J. A. *Ab Initio Molecular Orbital Theory*; John Wiley & Sons: New York, 1986.
(46) Becke, A. D. In *Exchange-Correlation Approximation in Density-Functional Theory*; Yarkony, D. R., Ed.; World Scientific: Singapore, 1995.
(47) Dewar, M. J. S.; Zoebisch, E. G.; Healy, E. F.; Stewart, J. J. P. *J. Am. Chem. Soc.* **1985**, *107*, 3902−3909.
(48) Stewart, J. J. P. *J. Comput. Chem.* **1989**, *10*, 209−221.
(49) Curtiss, L. A.; Redfern, P. C.; Smith, B. J.; Radom, L. *J. Chem. Phys.* **1996**, *104*, 5148−5152.
(50) McQuarrie, D. A. *Statistical mechanics*; Harper & Row: New York, 1976.
(51) *JAGUAR*, 4.2 ed.; Schrödinger, Inc.: Portland, OR, 1998.
(52) Frisch, M. J.; Trucks, G. W.; Schlegel, H. B.; Scuseria, G. E.; Robb, M. A.; Cheeseman, J. R.; Zakrzewski, V. G.; Montgomery, J. A.; Stratmann, R. E.; Burant, J. C.; Dapprich, S.; Millam, J. M.; Daniels, A. D.; Kudin, K. N.; Strain, M. C.; Farkas, O.; Tomasi, J.; Barone, V.; Cossi, M.; Cammi, R.; Mennucci, B.; Pomelli, C.; Adamo, C.; Clifford, S.; Ochterski, J.; Petersson, G. A.; Ayala, P. Y.; Cui, Q.; Morokuma, K.; Malick, D. K.; Rabuck, A. D.; Raghavachari, K.; Foresman, J. B.; Cioslowski, J.; Ortiz, J. V.; Stefanov, B. B.; Liu, G.; Liashenko, A.; Piskorz, P.; Komaromi, I.; Gomperts, R.; Martin, R. L.; Fox, D. J.; Keith, T.; Al-Laham, M. A.; Peng, C. Y.; Nanayakkara, A.; Gonzalez, C.; Challacombe, M.; Gill, P. M. W.; Johnson, B.; Chen, W.; Wong, M. W.; Andres, J. L.; Gonzalez, C.; Head-Gordon, M.; Replogle, E. S.; Pople, J. A. *Gaussian 98*, A.6 ed.; Gaussian Inc.: Pittsburgh, PA, 1998.
(53) Field, M. J. *A practical introduction to the simulation of molecular systems*; Cambridge University Press: Cambridge, UK, 1999.
(54) Field, M. J.; Albe, M.; Bret, C.; Proust-de Martin, F.; Thomas, A. *J. Comput. Chem.* **2000**, *21*, 1088−1100.

Scheme 2

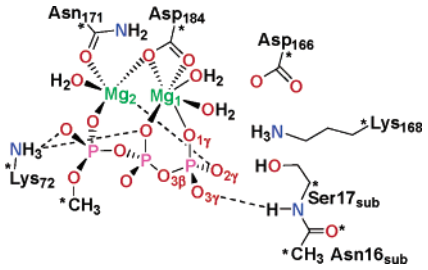

solvent molecules using the hybrid QM/MM AM1/OPLS-AA Hamiltonian implemented in the DYNAMO library.[54,55]

Once the cluster model of the kinase active site was constructed, we located various minima and transition structures on the B3LYP/6-31G* potential energy surface (PES)[46] using the Jaguar program.[51] During geometry optimizations, the Cβ atom of the kinase residues (Cϵ in the case of Lys_{72}), the Cα and O atoms of $Asn16_{sub}$, the Cα of $Ser17_{sub}$, and the C atom of the methyl triphosphate moiety were fixed at their initial positions to maintain the relative orientation of the cluster residues found in the X-ray structure (see Scheme 2). Transition structures were located by means of the synchronous transit guided quasi-Newton method[56] as implemented in the Jaguar program. To characterize the critical points located on the B3LYP/6-31G* PES, we carried out *numerical* frequency calculations. However, the large size of the cluster model (92 atoms and 789 basis functions) prevented us from carrying out full frequency calculations. For each optimized structure, we computed *partial* frequencies including the main reactive atoms (Asp_{166}−COO, Lys_{168}−NH_3, $Ser17_{sub}$−CH_2OH, ATP−Pβ−O3β−PγO$_3$, Mg_1, and Mg_2 in Scheme 2). Of course, this is essentially a compromise between computational cost and accuracy. However, by comparing analytical vs partial numerical frequency calculations on some small model systems, we found that the partial frequency calculations can predict reasonably well vibrational frequencies and normal mode motions as long as a judicious partitioning of the subsystem is used. After geometry optimization and frequency calculations, the electronic energies of the critical structures were refined by means of single-point B3LYP calculations using the 6-31+G** basis set.

To estimate the effect of the environment (protein and solvent) polarity on the different critical structures, we first performed single-point self-consistent reaction field (SCRF) calculations on the gas-phase QM geometries using the Poisson−Boltzmann solver included in Jaguar.[57] Several values for the dielectric constant of the surrounding continuum (ϵ) were considered so as to analyze the trend in the relative solvation energies: 80 (water, high polarity), 20 (intermediate polarity), and 4 (low polarity).

To gain insight into the *specific* electrostatic influence exerted by the PKA protein, we carried out simple electrostatic calculations of the first-order interaction energy between a set of Merz−Kollman (MK) charges[58] located on the QM atoms and the electrostatic potential created by the rest of protein atoms and the solvent continuum. Prior to the electrostatic calculations, the optimized critical points were rigidly docked into our starting structure for the kinase−substrates ternary complex followed by a partial AM1/OPLS-AA relaxation of the surrounding protein residues (e.g., the *flexible* glycine-rich turn). The electrostatic calculations were performed with the UHBD program[30] using a grid spacing of 0.4 Å and a dielectric constant of $\epsilon_{solvent} = 80.0$. To enable comparison with the SCRF calculations, which use a dielectric constant (ϵ) of 1 for the QM region, we performed the electrostatic calculations with an $\epsilon_{protein} = 1$, given that the UHBD program cannot handle two different dielectric constants in the protein region (one for the QM kinase active site and another for the rest of the protein).

The electronic nature of the breaking and forming P−O bonds for both reaction mechanisms was further analyzed in the context of the Theory of Atoms in Molecules developed by Bader,[59] by locating the corresponding bond critical points (BCPs) of the charge density $\rho(r)$. In principle, the values of $\rho(r_c)$, its Laplacian $\nabla^2\rho(r_c)$, and the local energy density $H(r_c)$[60] at a given BCP, enable one to characterize the interatomic interactions. The BCP analysis employed the EXTREME program, part of the AIMPAC suite of programs.[61]

Results

MD Simulation. To explore the conformational space of the prereactive complex of the cAMP-dependent protein kinase complexed with Mg_2ATP and a 20-residue peptide substrate, we computed an MD trajectory (~1.8 ns) of the fully solvated ternary complex. Analysis of the flexibility of the protein and substrates together with the characterization of the enzyme−ATP, enzyme−peptide, and peptide−ATP contacts provides information that is mechanistically relevant.

Protein Root Mean Square Deviation and Flexibility. The heavy atom RMS coordinate deviations (RMSDs) and the RMS coordinate fluctuations (RMSFs) of the simulated PKA complex relative to the 1CDK crystal structure and to the MD-average protein structure, respectively, are given in Table S1 of the Supporting Information. The bilobal catalytic core, which is conserved in the whole protein kinase family (residues 40−300 in PKA), displayed relatively low RMSD and RMSF values of 1.3 ± 0.0 Å and 0.8 ± 0.1 Å, respectively, which characterizes it as a stable and relatively rigid motif in PKA. In contrast, the RMSD and RMSF values of the nonconserved N- and C-terminal portions of the catalytic subunit are much higher, in agreement with the high-temperature factors observed in the crystal structure.

The fluctuations of the main catalytic motifs that directly bind the substrate molecules and contribute to the phosphoryl-transfer process are quite low: 0.5 ± 0.1 Å (link loop), 0.4 ± 0.1 Å (β-strand 3), 0.3 ± 0.0 Å (catalytic loop), and 0.4 ± 0.1 Å (Mg-positioning loop). Interestingly, the glycine-rich sequence and the activation loop are slightly more flexible according to their RMSF values (0.6 ± 0.1 Å and 1.0 ± 0.2 Å, respectively). More specifically, the RMSF values of the residues along the glycine-rich motif decrease from the base to the tip of the flap where Ser_{53} is quite rigid (RMSF = 0.1 ± 0.0 Å). However, Ser_{53} is clearly disordered in the crystal structures that lack the γ-phosphoryl group of ATP.[7] Thus, it is likely that the strong interaction between the backbone amino group of Ser_{53} and the terminal phosphoryl group of ATP that is observed in the prereactive complex (see below) will weaken during the phosphoryl-transfer reaction. As a result, the flexibility of the glycine-rich sequence will increase on going from the prereactive complex to the product complex, which could be a trigger event for product release.

Enzyme−Substrate Binding Determinants. The active site of protein kinases is located at the interface between the small

(55) Jorgensen, W. L.; Maxwell, D. S.; Tirado-Rives, J. *J. Am. Chem. Soc.* **1996**, *118*, 11225−11236.
(56) Peng, C.; Schlegel, H. B. *Isr. J. Chem.* **1994**, *33*, 449.
(57) Tannor, D. J.; Marten, B.; Murphy, R.; Friesner, R. A.; Sitkoff, D.; Nicholls, A.; Ringnalda, M.; Goddard, W. A., III; Honig, B. *J. Am. Chem. Soc.* **1994**, *116*, 11875−11882.
(58) Besler, B. H.; Merz, K. M. J.; Kollman, P. A. *J. Comput. Chem.* **1990**, *11*, 431−439.
(59) Bader, R. F. W. *Atoms in Molecules: A Quantum Theory*; Clarendon Press: Oxford, 1990.
(60) Grimme, S. *J. Am. Chem. Soc.* **1996**, *118*, 1529−1534.
(61) Biegler-Köning, F. W.; Bader, R. F. W.; Wang, T. H. *J. Comput. Chem.* **1982**, *3*, 317−328.

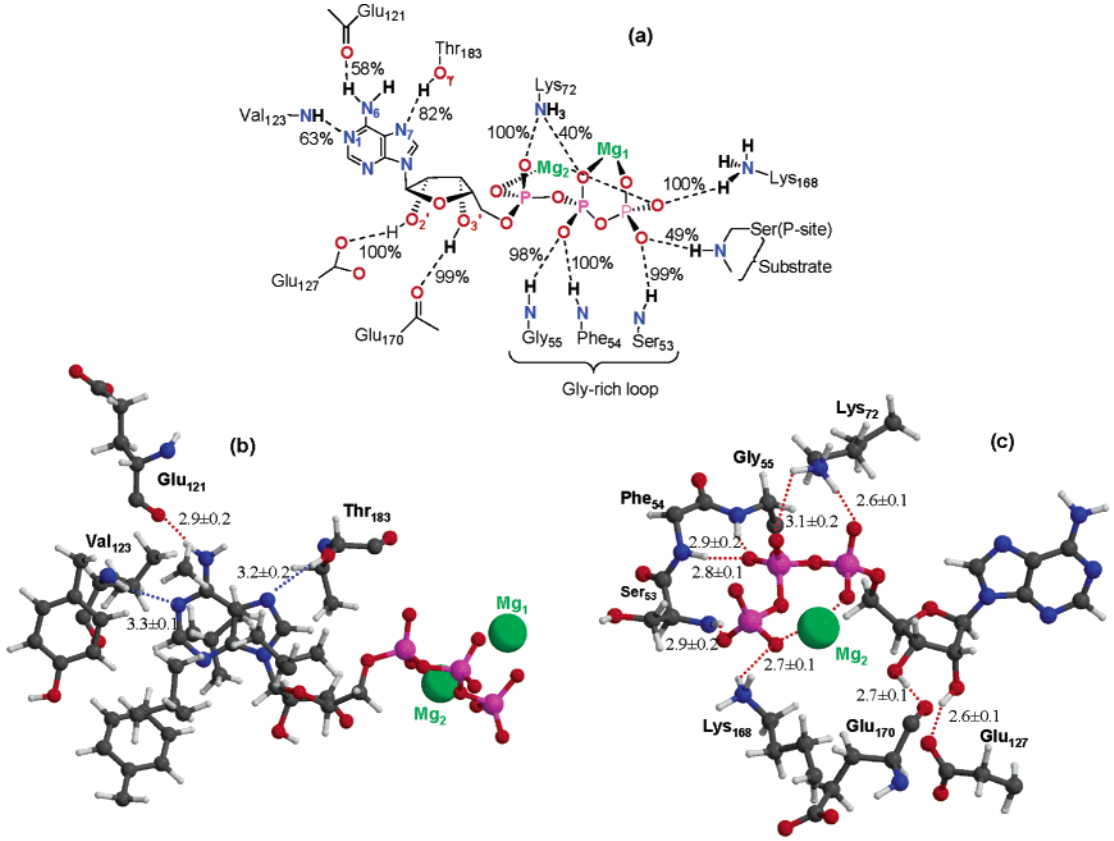

Figure 2. (a) Schematic representation of the most important polar interactions of the ATP molecule in the PKA active site. (b) Snapshot obtained along the MD simulation (950 ps) showing the main hydrophobic and polar interactions of the adenine ring and (c) the main polar interactions of the ribose ring and the triphosphate arm of ATP. For the sake of clarity, some backbone and side chain atoms are not represented. Distances between heavy atoms involved in H-bond interactions are given in angstroms. Figure produced with Molscript[8] and Raster3D.[9]

and large lobes that form the conserved core of the catalytic domain. In this active site, the essential magnesium ion is coordinated in an octahedral arrangement by the β- and γ-phosphates of ATP, the side chain of the invariant residue Asp_{184}, and two water molecules. The second low affinity metal ion is coordinated in a distorted octahedral geometry by the α-, β-, and γ-phosphates of ATP, the side chains of Asn_{171} and Asp_{184}, and one water molecule. The average distances corresponding to the Mg−ligand bonds along the MD trajectory and the X-ray distances are included in Table S2 of the Supporting Information. According to these values, we conclude that the coordination sphere of both metal ions, which were represented only by nonbonded parameters, is relatively well maintained all along the simulated trajectory.

A snapshot and a scheme illustrating the polar kinase-ATP interactions are given in Figure 2, whereas we present in Figure 3 the main kinase−peptide contacts. In Table S3 of the Supporting Information, the main hydrophobic contacts between kinase residues and both substrates (ATP and the 20-residue peptide) are described in terms of mean distances, whereas, in Table S4, the hydrogen-bond contacts are characterized in terms of average distances between heavy atoms and percentage of occurrence data.

During the MD simulation, the ATP molecule is held in the kinase active site cleft by means of specific and long-lived interactions that involve residues of both protein lobes. The adenine ring of ATP is enclosed in a hydrophobic pocket formed by residues of the small lobe (Leu_{49}, Val_{57}, and Ala_{70}), the large lobe (Leu_{173} and Thr_{183}), and the small linker segment (Val_{123}) which connects the two lobes. In addition, the adenine moiety interacts with the enzyme by means of three long hydrogen bonds (ATP−N7···HOγ−Thr_{183}, ATP−N1···HN−Val_{123}, and Glu_{121}−CO···HN6−ATP) (see Figure 2 and Table S4). The ribose hydroxyl groups and the triphosphate moiety of ATP interact with the enzyme by means of strong hydrogen bonds, the corresponding O···O/N distances being quite short and dynamically stable along the MD trajectory. For example, the ribose 2′-OH group forms a short H-bond (2.6 ± 0.1 Å and 100% occurrence) with the carboxylate side chain of Glu_{127} in the link segment, whereas the 3'-OH group interacts with the catalytic loop residue Glu_{170} (2.7 ± 0.1 Å and 99% occurrence). In addition, the triphosphate arm of ATP interacts with the two lobes. In the small lobe, Lys_{72} in β-strand 3 interacts closely with the α-phosphate group (2.6 ± 0.1 Å and 100% occurrence) and, to a lesser extent, with the β-phosphate group (3.1 ± 0.2 Å and 40.5% occurrence). Curiously, the interaction of the ATP α- and β-phosphate groups with Lys_{72} is more symmetric in the initial X-ray structure (N···O ≈ 3.0 Å). Another decisive interaction of ATP with the small lobe involves several backbone NH groups of the Gly-rich sequence (Ser_{53}, Phe_{54}, and Gly_{55}) which are connected with the β- and γ-phosphates. In the large lobe, Lys_{168} located in the catalytic loop binds the γ-phosphoryl group at the entrance to the active site (see Figure 2).

The peptide substrates that are recognized by PKA are characterized by the presence of two arginine residues in the P-2 and P-3 positions, where P is the phosphorylation site, and by the presence of a small hydrophobic residue in the P + 1

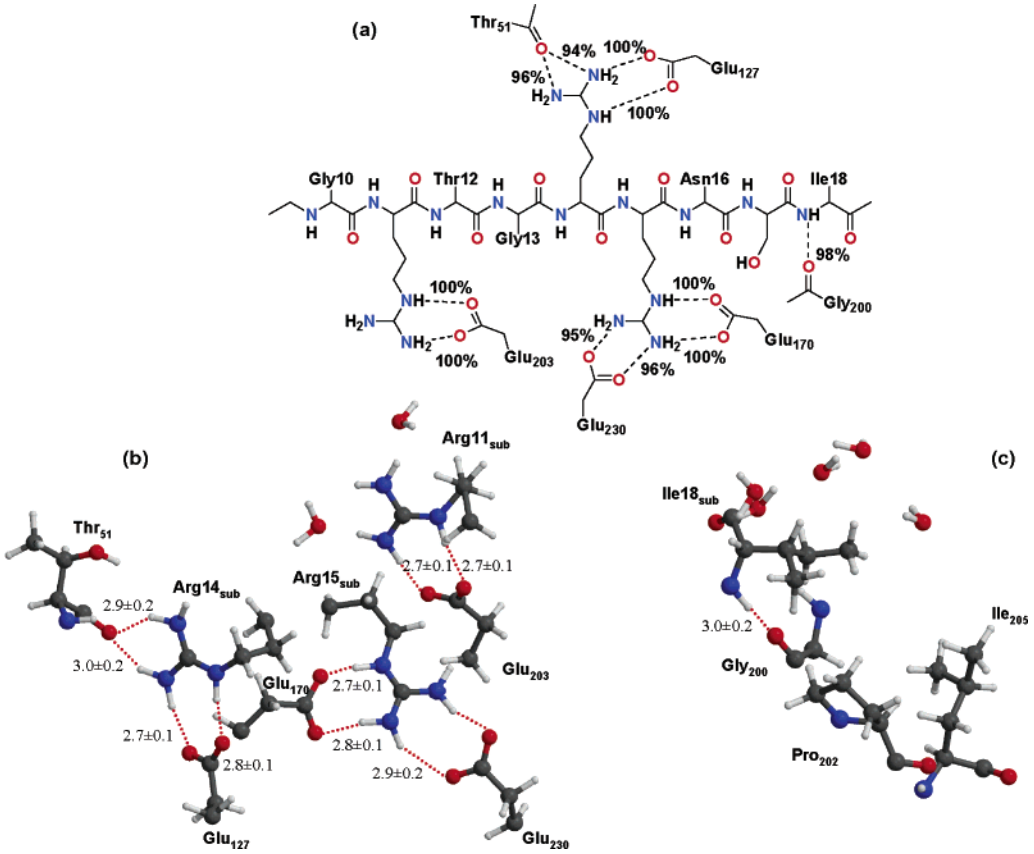

Figure 3. (a) Schematic representation of the most important interactions of the peptide substrate in the PKA active site. (b) Snapshot obtained along the MD simulation (950 ps) showing the main interaction of the P-2, P-3, and P-6 Arg residues of the substrate and (c) the main polar and hydrophobic interactions of the P + 1 Ile residue of the substrate. For the sake of clarity, some backbone and side chain atoms are not represented. Distances between heavy atoms involved in H-bond interactions are given in angstroms. Figure produced with Molscript[8] and Raster3D.[9]

position.[62] The guanidinium and backbone atoms of the P-6, P-3, and P-2 Arg residues and the carbonyl group of the P+1 Ile residue constitute important anchorage points between the peptide substrate and the PKA enzyme, which are dynamically stable throughout the simulation. The P-6, P-3, and P-2 Arg residues interact with an array of anionic PKA residues: Glu_{127} (in the extended coil connecting the two lobes), Glu_{170}, Glu_{203}, and Glu_{230} (in the large lobe). These interactions had 100% occurrence and average distances of 2.7−2.8 Å. In addition, the P-3 Arg also interacts with the backbone carbonyl group of Thr_{51} in the glycine-rich sequence (see Figure 3). Most remarkably, we note that the interaction between the backbone carbonyl group of the P-2 Arg and the side chain of Lys_{168}, which is observed in the initial X-ray structure, is rapidly lost at the beginning of the simulation. Thus, the Lys_{168} side chain moves to form a direct salt bridge with the carboxylate group of Asp_{166}, whereas the P-2 carbonyl group interacts through a long-lived *water bridge* with the O3γ atom of ATP ($Arg15_{sub}$−CO···H−O−H···O3γ−ATP, H-bond occurrences of 100% and 98.8%, respectively). This novel contact between the ATP γ-phosphoryl group and a bulk water molecule could be relevant for the ATPase activity (i.e., *water* as the nucleophile) exhibited by the catalytic subunit of PKA in the presence of peptide substrates but absent in the presence of inhibitors. On the other hand, the backbone amino group of the isoleucine at the P + 1 position interacts with the carbonyl group of Gly_{200} (3.0 ± 0.2 Å and 97.6% occupancy). In addition, the hydrophobic side chain of this P + 1 residue partially lies in the hydrophobic environment provided by the side chains of Pro_{202} and Leu_{205} (see Table S3 in the Supporting Information).

Globally, it turns out that the serine nucleophile is firmly positioned in the kinase active site by means of salt-bridge contact pairs, hydrogen bonds, and hydrophobic interactions that mainly involve the residues of the peptide consensus sequence R−R−X−S−Hyd (where X is variable and Hyd is a hydrophobic residue).

Prereactive Contacts. Clearly, the H-bond contacts involving the nucleophilic hydroxyl and backbone groups of the P-site serine residue ($Ser17_{sub}$) are mechanistically relevant. In our simulation, $Ser17_{sub}$ interacts simultaneously with the ATP molecule and with the enzyme. Thus, the backbone amino group of $Ser17_{sub}$ is oriented toward the γ-phosphoryl of ATP, although this H-bond interaction (3.3 ± 0.2 Å and 47% occurrence) is slightly weaker compared with that observed in the initial X-ray structure (3.1 Å). This fact could be related to the side chain of the P-site serine which is bulkier than that of the alanine present in the enzyme−AMP-PNP−inhibitor crystallographic structure. The backbone carbonyl group of $Ser17_{sub}$ interacts through a quite stable H-bond with the hydroxyl group of Ser_{53} located at the tip of the Gly rich flap (2.8 ± 0.2 Å and 99.3% of occurrence) thereby contributing to the above-mentioned low flexibility of this residue.

Most interestingly, the P-site serine hydroxyl group interchanges rapidly between two conformations during the simula-

(62) Kemp, B. E.; Graves, D. J.; Benjamini, E.; Krebs, E. G. *J. Biol. Chem.* **1977**, *252*, 4888−4894.

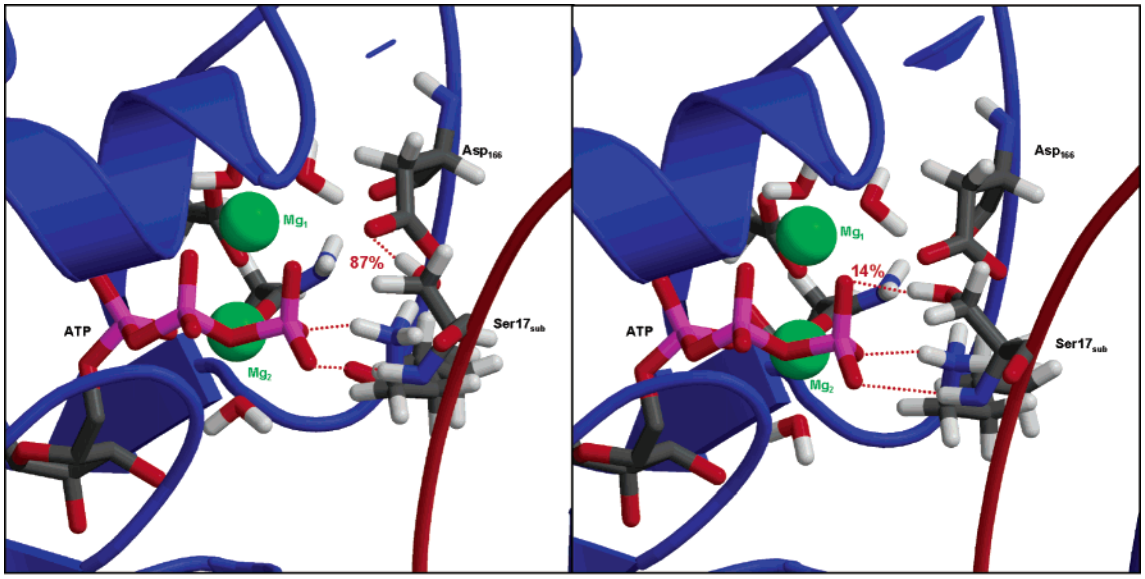

Figure 4. Snapshots showing the most significant prereactive contacts of the nucleophilic serine hydroxyl group along the simulated trajectory. Figure produced with Molscript[8] and Raster3D.[9]

tion. One conformation shows an $Ser17_{sub}-O\gamma H\cdots OOC-Asp_{166}$ H-bond, and the second one, an $Ser17_{sub}-O\gamma H\cdots O1\gamma-ATP$ contact (see Figure 4). The H-bond interaction with the Asp_{166} side chain (2.7 ± 0.2 Å and 87.0% occurrence) is shorter than that with the O1γ atom of ATP (3.2 ± 0.2 Å and 14.4% occurrence). The relative free energy of both conformers can be directly estimated from the population of each conformer (N_{ASP} and N_{ATP}) along the MD simulation by using the following equation:

$$\Delta G = -RT \ln\left(\frac{N_{ASP}}{N_{ATP}}\right)$$

which results in a small ΔG value of about ~1 kcal/mol favoring the contact with the carboxylic side chain of Asp_{166}. Finally, the average reaction coordinate distance between the entering oxygen atom and the γ-phosphorus of ATP ($Ser17_{sub}-O\gamma\cdots P\gamma-ATP$) amounts to 3.8 ± 0.3 Å. It is interesting to note that our average value for the $ATP-P\gamma\cdots O\gamma-Ser17_{sub}$ distance supersedes those previously obtained from *static* molecular modeling (2.7−3.0 Å),[19,28] all of which are clearly too short. Longer reaction coordinate distances of ~5 Å have been indirectly estimated by NMR measurements[63] and from crystal structures.[64,65] However, these larger values are not directly comparable with the 3.8 Å value obtained from our MD simulation because they were measured in a nonreactive system with nonphysiological metal ions located at the kinase active site ($PKA\cdots Mn^{2+}\cdots Cr^{3+}\cdots AMP-PCP$)[63] or from the crystal structures of other enzymes (insulin receptor tyrosine kinase) where the triphosphate arm of ATP is oriented in a different way compared with PKA.[64,65]

QM Calculations. A. Relative Performance of QM Levels of Theory. To validate the B3LYP/6-31G* geometries and B3LYP/6-31+G**//B3LYP/6-31G* energies to be used in the study of the cluster model of the PKA active site, we evaluated the proton affinity (PA) of the acetate anion as well as that of the methyl phosphate dianion at different levels of theory, including the additive G2(MP2,SVP) scheme[49] which approximates the sophisticated QCISD(T)/6-311+G(3df,2p) level of theory. The resulting equilibrium geometry and proton affinities of these systems are included in the Supporting Information. With respect to the molecular geometries, the ab initio and DFT results are quite close, whereas semiempirical geometries deviate from the ab initio ones, mainly because of the interaction of the phosphate dianion with the Mg^{2+} cations.

The computed PA of acetate at the G2(MP2,SVP) level of theory (347.0 kcal/mol) matches well the experimental values (343−348 kcal/mol).[66] Similarly, the B3LYP/6-31+G**// B3LYP/6-31G* and B3LYP/6-31+G** PAs of acetate (345.6) lie also within the experimental PA range. Concerning the semiempirical methods, the experimental heat of formation of the proton ($\Delta H_f(H^+)$ = 365.7 kcal/mol) is used in the PA calculations.[67] For the acetate anion, PM3 provides the best PA value (348.0 kcal/mol), whereas the AM1 one (353.3 kcal/mol) is close to the measured PA range. For the methyl phosphate dianion complexed with zero, one, or two Mg^{2+} cations, the B3LYP method with the 6-31+G** basis set provides PA values that are quite close to the G2(MP2,SVP) ones (±1−4 kcal/mol). In contrast, the two semiempirical methods (AM1 and PM3) give PA values for the $CH_3OPO_3^{2-}$ and $[Mg_2(CH_3OPO_3)]^{2+}$ species that differ from the G2(MP2,SVP) reference values by 18−27 kcal/mol in absolute value.

We also studied the gas-phase hydrolysis of methyl phosphate dianion by locating a TS for the nucleophilic substitution in the gas phase of a water molecule toward the P atom (see the Supporting Information). The optimized TS in the gas phase is largely dissociative (82%)[68] and determines energy barriers with respect to the prereactive $CH_3OPO_3^{2-}\cdots H_2O$ complex of 50.6,

(63) Granot, J.; Mildvan, A. S.; Bramson, H. N.; Kaiser, E. T. *Biochemistry* **1980**, *19*, 3537−3543.
(64) Hubbard, S. R. *EMBO J.* **1997**, *16*, 5572−5581.
(65) Parang, K.; Till, J. H.; Ablooglu, A. J.; Kohanski, R. A.; Hubbard, S. R.; Cole, P. A. *Nat. Struct. Biol.* **2001**, *8*, 37−41.
(66) *NIST Chemistry WebBook, NIST Standard Reference Database Number 69*; National Institute of Standards and Technology: Gaithersburg MD, March 2003.
(67) Dewar, M. J. S.; Dieter, K. M. *J. Am. Chem. Soc.* **1986**, *108*, 8075−8086.
(68) Mildvan, A. s. *Proteins: Struct., Funct., Genet.* **1997**, *29*, 401−416.

Table 1. Relative Energies (kcal/mol), with Respect to the Most Stable Prereactive Complex, of the Critical Structures Located for the Two Mechanisms (**A** and **B**) Studied in a Cluster Model of the PKA Active Site

			$\Delta\Delta G_{solv}$ B3LYP/6-31G* SCRF [a]			
structure	B3LYP/6-31G*	B3LYP/6-31+G** [a]	$\epsilon = 80.$	$\epsilon = 20$	$\epsilon = 4.0$	V_{Int} $\sum q_i^{MK} V_{elec,i}^{PB}$
CA	0.0	0.0	0.0	0.0	0.0	0.0
TS_1-A	16.5	17.2	−1.6	−1.4	−0.8	−0.1
Min_1-A	14.8	15.8	−5.8	−5.2	−3.9	−0.7
TS_2-A	20.2	22.8	−5.5	−5.1	−3.3	1.3
Min_2-A	15.2	16.7	−3.7	−3.4	−2.3	0.5
CB	2.1	2.6	−0.7	−0.6	−0.3	−0.7
TS_1-B	48.6	49.8	−1.0	−1.0	−0.8	−1.2
Min_1-B	33.7	33.8	−1.9	−2.0	−1.7	−1.5

[a] Single-point calculations at the gas-phase B3LYP/6-31G* geometries.

49.6, and 48.9 kcal/mol at the G2(MP2,SVP), B3LYP/6-31G+G**//B3LYP/6-31G*, and B3LYP/6-31+G** levels of theory, respectively. However, both AM1 and PM3 semiempirical methodologies strongly underestimate the energy barrier for this process by around 40 kcal/mol.

Overall, the B3LYP/6-31+G* level of theory gives proton affinities and relative energies close to the G2(MP2,SVP) values. Therefore, the results obtained from the test calculations support the use of the B3LYP/6-31G* level of theory in the optimization of the large cluster model of the PKA active site followed by single-point energy calculations at the B3LYP/6-31+G** level of theory in order to refine the computed energies.

B. Phosphoryl Transfer Step: QM Calculations on the Cluster Model. As previously mentioned, we investigated the molecular details of the phosphoryl-transfer event that takes place in the active site of protein kinases by considering a cluster model of the X-ray active site of PKA. Geometrical restrictions were applied in the search for PES critical points in order to preserve the relative orientation of the different residues near to their experimental X-ray conformation. In this respect, experimental evidence confirms that the formation of the TS for the nucleophilic substitution does not entail any significant structural changes with respect to the prereactive complex.[69]

Two mechanisms were located on the B3LYP/6-31G* PES which differ in the role played by the conserved Asp_{166} side chain along the reaction coordinate. The first mechanism (**A**) has a high degree of dissociative character, whereas the second one (**B**) is much less dissociative. The geometries of the critical structures are shown in Figures 5 and 6 for mechanisms **A** and **B**, respectively, whereas the corresponding relative electronic energies with respect to the most stable prereactive complex located on the PES are given in Table 1. Unless otherwise noted, energies given in the text correspond to the single-point B3LYP/6-31+G** calculations on the B3LYP/6-31G* geometries.

Mechanism **A** starts at a prereactive complex (**CA** in Figure 5) in which the O atom of the nucleophilic hydroxyl group of the $Ser17_{sub}$ side chain is 3.9 Å away from the P atom of the terminal phosphoryl group (γ-phosphoryl group of ATP). We note that this value is quite close to the reaction coordinate distance obtained from the MD simulation of the ternary reactive complex. In addition, the hydroxyl group interacts with the carboxylate group of the essential Asp (Asp_{166} in PKA) through a short H-bond (O···O distance of 2.7 Å). Other noncovalent contacts in the cluster model are similar to those present in the initial X-ray structure. Thus, the amino backbone of the reactive serine interacts with the O3γ atom of the methyl triphosphate moiety (O3γ···HN 1.9Å), whereas the ammonium side chain of Lys_{168} interacts with the O2γ atom of the terminal phosphoryl group (O2γ···H−Nζ 1.8 Å).

Clearly, the relative orientation of the nucleophilic OH and the terminal phosphoryl group as well as the H-bond contact with the carboxylate group observed in **CA** are favorable for a nucleophilic displacement with simultaneous proton transfer from the hydroxyl to the carboxylate group. These reactive events can take place passing through the **TS_1-A** structure (see Figure 5). Remarkably, proton transfer at **TS_1-A** is only in its initial stage (O_{ser}−H = 1.0 Å and O_{ser}···Oδ2 = 2.5 Å), whereas the O3β−Pγ bond is already markedly broken (2.4 Å) and the Pγ−O_{ser} bond is significantly formed (2.0 Å). Hence, we can consider that **TS_1-A** has a high degree of dissociative character (84% using Pauling's formula as suggested by Mildvan[68]) showing that the proton can be transferred to the Asp side chain in a concerted fashion with the nucleophilic substitution. Frequency calculations confirm that the transition vector at **TS_1-A** ($\nu \approx 118$ i cm^{-1}) has a small contribution from movement of the serine hydroxyl hydrogen. The transition vector is dominated by a torsional movement of the carboxylate side chain of Asp_{166} and a movement of the ammonium group of Lys_{168} concomitant with the nucleophilic displacement. Energetically, **TS_1-A** has a barrier of 17.2 kcal/mol with respect to **CA**.

TS_1-A evolves to a minimum (**Min_1-A** in Figure 5) in which the γ-phosphoryl group is transferred to the serine side chain (Pγ−O_{ser} 1.75 Å). In this structure, the protonated Asp side chain interacts closely with the serine Oγ atom through a short H-bond with an O···O distance of 2.6 Å. This minimum is structurally close to the **TS_1-A** critical point and is only 1.4 kcal/mol below it in energy (15.8 kcal/mol above **CA**).

Min_1-A can evolve through a second transition structure (**TS_2-A** in Figure 5) whose transition vector is mainly dominated by the rotation of the protonated Asp moiety ($\nu \approx 304$ i cm^{-1}). In **TS_2-A**, the Asp−COOH group establishes a bifurcated H-bond with the serine Oγ atom (O−H···O_{ser} distance of 1.9 Å) and with the O2γ atom of the transferred phosphoryl group (O−H···O2γ distance of 1.9 Å). **TS_2-A** has an energy barrier of 22.8 kcal/mol, 5.6 kcal/mol higher than the barrier corresponding to the phosphoryl-transfer step. After passing **TS_2-A**, a second proton transfer occurs as the Asp-COOH group donates its proton to the O2γ atom of the phosphorylated substrate and produces the **Min_2-A** critical structure. The resulting Asp−

(69) Madhusudan; Akamine, P.; Xuong, N.; Taylor, S. S. *Nat. Struct. Biol.* **2002**, *9*, 273−277.

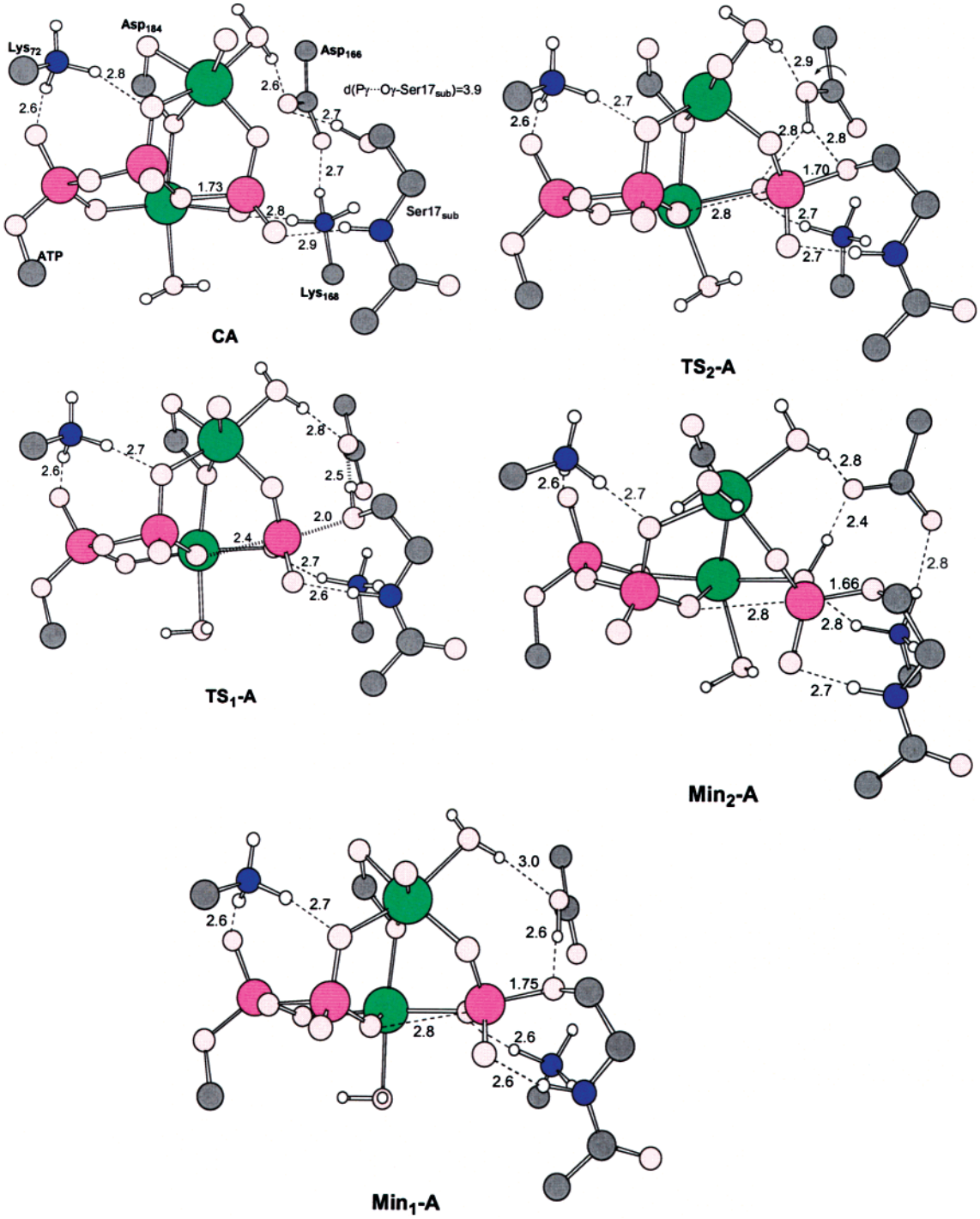

Figure 5. B3LYP/6-31G* critical structures located along the Asp-assisted phosphoryl-transfer reaction (mechanism **A**). Distances between heavy atoms are given in angstroms. For the sake of clarity, Asn_{171}, the Cβ, Cγ, and Cδ atoms of Lys_{168}, the Cβ atom of Asp_{184}, and some H atoms are not represented.

COO^- and $Ser-O-PO_3H^-$ groups interact strongly via a short $O2\gamma-H\cdots O$ H-bond (1.4 Å). Energetically, **Min$_2$-A** is 0.9 kcal/mol less stable than **Min$_1$-A**. However, given that the geometrical constraints required to preserve the overall architecture of the cluster model are appropriate for the initial stages of the phosphoryl-transfer event (i.e., **CA** → **TS$_1$-A** → **Min$_1$-A**) and that both **TS$_2$-A** and **Min$_2$-A** exhibit a significant rearrangement of charged groups with respect to **CA**, it is possible that the relative energies of **TS$_2$-A** and **Min$_2$-A** are overestimated by a few kcal/mol.

The second mechanism (**B**) for phosphoryl transfer which was characterized on the B3LYP/6-31G* PES starts at the prereactive complex **CB** shown in Figure 6. In **CB**, the nucleophilic serine side chain interacts with one of the oxygen atoms of the γ-phosphoryl group of ATP ($O1\gamma\cdots O_{ser}$ distance of 2.8 Å). Other interactions in **CA** and **CB** are similar although the reactive $P\gamma\cdots O_{ser}$ distance for nucleophilic displacement in **CB** is quite short (3.4 Å). Energetically, **CB** is slightly less favored than **CA** by 2.6 kcal/mol, in reasonable agreement with the relative population of prereactive conformers observed along the MD trajectory.

The prereactive complex **CB** can evolve through a TS for phosphoryl transfer (**TS$_1$-B** in Figure 6) with simultaneous protonation of the forming phosphorylated group. Geometrically,

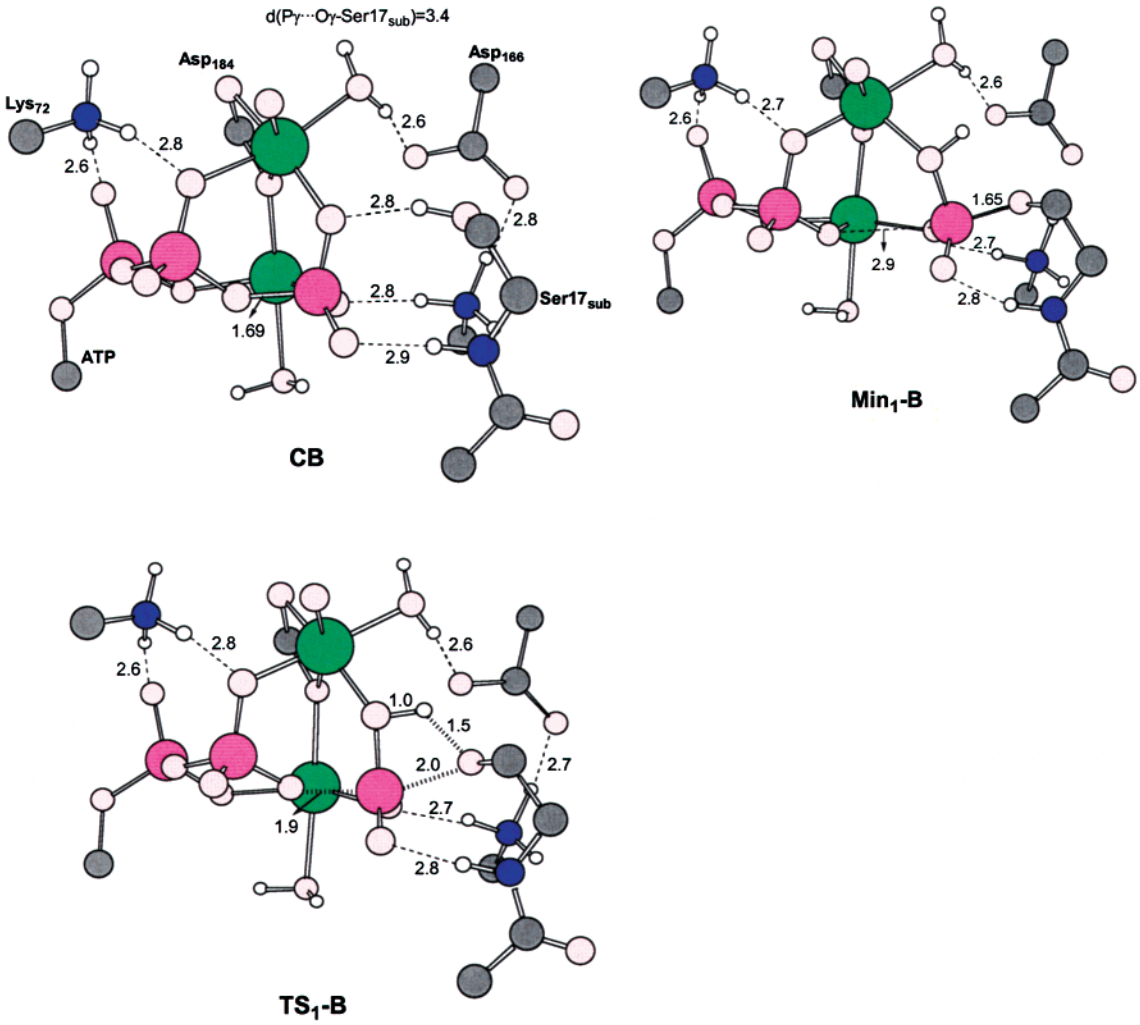

Figure 6. B3LYP/6-31G* critical structures located along the phosphoryl-transfer reaction with direct proton transfer to the γ-phosphoryl group (mechanism **B**). Distances between heavy atoms are given in angstroms. For the sake of clarity, Asn_{171}, the Cβ, Cγ, and Cδ atoms of Lys_{168}, the Cβ atom of Asp_{184}, and some H atoms are not represented.

the forming P$\gamma-O_{ser}$ distance at **TS_1-B** coincides with that at **TS_1-A** (2.0 Å), whereas the breaking O3$\beta-$Pγ distance is 1.9 Å at **TS_1-B** and 2.4 Å at **TS_1-A**. Hence, the lower dissociative character of **TS_1-B** (62%) compared with **TS_1-A** is determined by the different degree of leaving group departure. In addition, the H atom of the nucleophilic hydroxyl group is practically transferred to the O1γ oxygen atom of the γ-phosphoryl group (O1$\gamma-$H = 1.0 Å). The transition vector at **TS_1-B** ($\nu \approx 311$ i cm^{-1}) has a large contribution from movement of the transferred hydrogen atom that accompanies the inversion of configuration at Pγ during the nucleophilic substitution. Energetically, **TS_1-B** is 49.8 kcal/mol less stable than the prereactive complex **CA** (32.6 and 27.0 kcal/mol above **TS_1-A** and **TS_2-A**, respectively). The high energy barrier associated with **TS_1-B** may be related to its higher *associative* character which, in turn, determines a strained conformation of the reacting atoms. This strained conformation in **TS_1-B** is well illustrated by several acute bond angles ($H_{ser}-$O1$\gamma-$Pγ = 92°, O1$\gamma-$P$\gamma-O_{ser}$ = 75°, P$\gamma-O_{ser}-H_{ser}$ = 66°). In contrast, the more dissociative character of **TS_1-A** and the absence of the four-membered ring for the H-shift process can explain the large energy difference between the **TS_1-A** and **TS_1-B** critical structures for the phosphoryl-transfer event.

TS_1-B is connected to the minimum **Min_1-B** (see Figure 6) in which the γ-phosphoryl group is completely transferred to the serine side chain (P$\gamma-O_{ser}$ = 1.65 Å and a P$\gamma\cdots$O3β = 2.9Å) without dramatically distorting other interactions present in the previous **CB** and **TS_1-B** structures. This minimum is 33.8 kcal/mol above **CA** which suggests that protonation of the oxygen atom which interacts with the high affinity Mg^{2+} ion is energetically unfavorable.

In the product complexes obtained for the phosphoryl-transfer reaction (**Min_1-A**, **Min_2-A**, and **Min_1-B**), the optimized O3$\beta\cdot\cdot\cdot$Pγ distances (2.8−2.9 Å) are lower than the corresponding van der Waals distance (3.3 Å) which might suggest an incomplete O$\cdots$P bond breakage. To assess this possibility, we characterized the P$\cdots$O interatomic interaction by analyzing the properties of the corresponding O3$\beta\cdots$Pγ BCP using the tools of the Theory of Atoms in Molecules.[59] The main results from this analysis, collected in Table S5 of the Supporting Information, indicate that the O3β and Pγ atoms establish only a very weak closed-shell interaction (i.e., noncovalent) in **Min_1-A** and **Min_2-A**, whereas they do not interact in **Min_1-B**. Therefore, we conclude that the phosphoryl-transfer process has been effectively completed in our product complexes.

C. Environmental Effects. In principle, the energy difference

between the two phosphoryl-transfer TSs (**TS_1-A** and **TS_1-B**) is large enough (32.6 kcal/mol) for environmental effects not to reverse the energetic preference for the more dissociative mechanism assisted by the Asp_{166} side chain. To check this hypothesis, we first performed single-point self-consistent reaction field (SCRF) energy calculations on the gas-phase QM geometries using three different values for the dielectric constant of the surrounding continuum ($\epsilon = 80$, 20, and 4). The relative solvation energies ($\Delta\Delta G_{solv}$) obtained from these calculations are included in Table 1. The moderate values of the relative solvation energies (~ -1, -5 kcal/mol) obtained with the high-, medium-, and low-dielectric constants show that the polarity of the protein−solvent environment cannot modify significantly the gas-phase energy barriers.

Taking into account that protein−solvent environments are not homogeneous media characterized by a single dielectric constant, we decided to estimate the electrostatic impact of the environment along the reaction profile using a point-charge representation of the protein coupled with a solvent continuum model. To this end, we carried out Poisson−Boltzmann electrostatic calculations of the first-order interaction energy between a set of DFT MK charges representing the QM structures and the electrostatic potential created by the rest of the protein atoms and the solvent continuum. Prior to these calculations, the optimized QM clusters were rigidly docked into the initial model of the kinase tertiary complex. AM1/OPLS-AA energy minimizations were performed to relax several contacts mainly involving the flexible Gly-rich sequence which covers the ATP molecule in the active site. The resulting electrostatic interaction energy differences along both pathways were quite low, ~ -1 to 2 kcal/mol (see the V_{int} values collected in Table 1). Based on the small magnitude of these classical V_{int} electrostatic energies and the QM-SCRF relative solvation energies, we conclude that most probably environmental effects are not going to reverse the energy preference for the most dissociative mechanism.

Discussion

In the present work, we have performed an MD simulation of a ternary complex made up of the catalytic subunit of cAMP-dependent protein kinase, Mg_2ATP, and a 20-residue peptide substrate. The simulation allowed us to characterize in aqueous solution the dynamical stability of important catalytic motifs and the main enzyme−substrate contacts present in the prereactive complex. It is interesting to note that although previous crystallographic studies provided very valuable structural information on binary and ternary complexes with inhibitors, substrate analogues, TS analogues, or products, a detailed picture of the kinase−ATP and kinase−peptide contacts in a prereactive situation has been unavailable. Moreover, the interactions displayed by the P-site serine residue in the prereactive ternary complex are mechanistically relevant and can shed additional light on proposals inferred from the crystal structures.

The chemical reaction catalyzed by protein kinases involves the transfer of the terminal γ-phosphoryl of ATP to the hydroxyl side chain of serine, threonine, or tyrosine residues in different peptide substrates. This process is accompanied by (at least) one hydrogen transfer from the nucleophilic hydroxyl group to one acceptor atom. Whether this H atom goes directly to one of the oxygen atoms of the ATP molecule or passes to a kinase residue (e.g., Asp_{166} in PKA) is still an open question.

The carboxylate group of Asp_{166} in the cAMP-dependent protein kinase is a candidate to accept the hydroxyl hydrogen atom of the nucleophilic serine side chain. The presence of this anionic residue in the active site of all protein kinases so far identified highlights its catalytic relevance. Thus, an X-ray crystal structure of a ternary complex among the catalytic subunit of PKA, ADP, and a peptide substrate suggests the existence of an H-bond interaction between the P-site serine side chain and the invariant aspartate (O···O distance $\approx$ 2.7Å).[19] In addition, the recently reported crystal structure of a TS analogue (ADP···AlF_3···Ser−substrate) complexed to PKA assigns a distance of 2.5 Å to the Ser−Oγ···OOC−Asp_{166} contact.[69] On the other hand, substitution of the Asp_{166} homologue in yeast PKA by alanine produces a mutant enzyme with a residual catalytic activity of 0.4% with respect to the wild-type enzyme (370-fold decrease in k_{cat}).[20] Overall, both structural and kinetic results are considered compatible with the participation of Asp_{166} as a base catalyst in the phosphoryl-transfer mechanism.

Arguments against the base-catalyst hypothesis arise from analysis of the pH and kinetic solvent isotope effects on k_{cat} and on the "burst" phase of the PKA catalyzed reaction. Thus, no pH dependence was observed either on k_{cat} or on the "burst" rate constant within the pH range 6−9.[15] These results indicate that a hypothetical base catalyst should have a pK_a lower than 5. In this scenario, the basic strength of the Asp_{166} residue in PKA would be low, and therefore, it would not be an effective base catalyst to deprotonate the nucleophilic serine in the enzyme ground state. In addition, no solvent isotope effect was measured for the "burst" phase of the reaction, which was found incompatible with a transition state in which the hydroxyl H atom is being abstracted by the base catalyst.[15]

Initial theoretical work has not supported the base-catalyst hypothesis either. According to *semiempirical* QM and QM/MM calculations,[23,24] the reaction pathway in which the Asp_{166} side chain becomes protonated is energetically much less favorable ($\sim$11 kcal/mol) than a reaction mechanism in which the hydroxyl proton is directly transferred to one of the oxygen atoms of the γ-phosphoryl moiety of ATP. However, it must be noted that the rate-determining TSs reported in these studies are clearly dominated by the serine hydroxyl H-shift, in sharp contrast with the above-mentioned absence of solvent isotope effects on the burst phase of the reaction. Moreover, our test calculations summarized in the Supporting Information point out that semiempirical calculations do not account well for the relative intrinsic basicity of carboxylate and phosphate groups as compared to either B3LYP or G2(MP2,SVP) calculations.

Let us analyze now if our molecular simulations can aid in the interpretation of previous experimental results. According to the MD simulation of the prereactive complex formed by PKA, Mg_2ATP, and a 20-residue peptide substrate, the interaction between the P-site serine hydroxyl and the Asp_{166} carboxylate groups is dynamically stable, in good agreement with the available X-ray structure.[19] Moreover, the relatively short average O···O distance of the Ser−OγH····$^-$OOC−Asp_{166} contact (2.7 $\pm$ 0.2 Å) clearly suggests an active catalytic role for the conserved Asp_{166} residue, as observed by mutagenesis experiments. Thus, the proposal in which the Ser−OγH····$^-$OOC−Asp_{166} interaction could promote phosphoryl transfer by limiting the number of hydroxyl rotamers and positioning the

nucleophile for productive substitution on the γ-phosphoryl group of ATP[15] is certainly supported by our MD simulation. Nevertheless, positioning the nucleophile cannot be the unique kinetic role played by Asp_{166} as revealed by site-directed mutagenesis of Asp_{149} in phosphorylase kinase (the analogue to Asp_{166} in PKA).[70] In this case, the Asp149Ala and Asp149Asn mutants showed dramatic decreases in k_{cat} (1.3×10^4 and 4.7×10^3, respectively). Although the Asn_{149} side chain in the mutant enzyme might fulfill the orientation function played by the Asp residue in the wildtype enzyme, it is a much poorer proton acceptor than Asp. This could explain the significant decrease (possibly as great as 2.2×10^3) in the rate constant characterizing the chemical step.

Our DFT study of the reaction mechanisms in the cluster model of the PKA active site and the results reported by Valiev et al. in their parallel study[27] clearly point out that the Asp_{166} side chain can have an active kinetic role besides orienting the nucleophile. In effect, at the energetically most favorable TS for the phosphoryl-transfer event, the Asp_{166} carboxylate group is ready to accept the hydroxyl H atom from the P-site serine side chain through an $Ser_{sub}-O\gamma H\cdots{}^{-}OOC-Asp_{166}$ contact (See **TS_1-A** in Figure 5). This transition structure is characterized by the advanced cleavage of the ATP $O3\beta-P\gamma$ bond (2.4 Å) and a moderate degree of $P\gamma\cdots O-Ser_{sub}$ bond formation (2.0 Å) which results in a dissociative character of 84%. Most interestingly, the serine hydroxyl H atom has not been transferred to the Asp_{166} side chain at **TS_1-A** ($O\gamma-H$ distance of 1.0 Å) in agreement with the absence of solvent isotope effects on the "burst" phase of the reaction (see above). After passing through **TS_1-A** downhill on the PES to the **Min_1-A** structure, bond making between the γ-phosphoryl group and the serine side chain progresses, the acidity of the serine hydroxyl group increases, and proton delivery from the hydroxyl to the carboxylate group takes place without additional energy cost. Energetically, the gas-phase energy barrier determined by **TS_1-A** amounts to 17.2 kcal/mol which compares reasonably well with the $k_{transfer}$ rate constants of $500-154 s^{-1}$ measured for the burst phase of the reactions with different substrates[15,71] (the experimental $\Delta G^{\ddagger}$ would be ~14−15 kcal/mol according to the general transition state theory). Moreover, the X-ray structure of PKA complexed with the TS-analogue $ADP\cdots AlF_3\cdots Ser_{sub}$ shows an $Asp_{166}-COO^{-}\cdots O\gamma-Ser_{sub}$ contact of 2.5 Å,[69] which is very close to that observed in the **TS_1-A** structure (2.6 Å, see Figure 5). In this paper, the authors also observed a change of >20° in the χ^2 angle of the Asp_{166} side chain of PKA complexed with peptide substrates/inhibitors compared to the structure complexed with the TS analogue (from 25−20° to −1.5°). A similar magnitude for this torsion angle change is observed in our cluster model on going from **CA** to **TS_1-A**. Thus the χ^2 angle of the Asp_{166} side chain was qualitatively estimated after docking and partial relaxation of **CA**, **CB**, **TS_1-A**, and **TS_1-B** in the initial PKA structure. Comparing **CA** and **TS_1-A**, a change of ~30° is observed in this angle (from −8.5° to −38.9°), whereas χ^2 remains almost the same in **CB** and **TS_1-B** (19.2° and 18.6°, respectively). As a result, **TS_1-A** is structurally close to the crystal structure of PKA when complexed with the TS-analogue $ADP\cdots AlF_3\cdots HO\gamma-Ser_{sub}$.

Although the structure (85% dissociative character) and energy barrier (11 kcal/mol) of the transition state reported by Valiev et al.[27] are similar to those of our **TS_1-A** structure, their corresponding product complex turns out to be 9 kcal/mol more stable than their prereactive complex. Intriguingly, the high stability of this product complex contrasts sharply with the relative energies obtained for **Min_1-A** and **Min_2-A** in the present work. However, we note that Valiev et al. did not include in their model the two water molecules that coordinate the high affinity magnesium ion (Mg_1 in Scheme 2). As a consequence, the Mg_1 ion in the Valiev et al. product complex interacts closely with the $O3\beta$ atom of the ADP moiety (2.2 Å), whereas, for their prereactive complex and transition state, the corresponding $Mg_1\cdots O3\beta$ distances are 3.0 and 2.6 Å, respectively. [27] In contrast, in our cluster models, the $Mg_1\cdots O3\beta$ distances are 3.1−3.2 Å all along the reaction coordinate, similar to the $Mg_1\cdots O3\beta$ distances observed in the crystal structures of PKA complexed with substrate and TS analogues (3.2−3.3 Å). Hence, the stability of the product complex of Valiev et al. is most likely overestimated due to the extra $Mg_1\cdots O3\beta$ interaction.

Clearly, the cluster models studied in this work give only a partial insight into the molecular events that take place during the regeneration of the active site. Nevertheless, it is interesting to note that, according to our calculations, the energy difference between the product complex with phosphorylated-serine and protonated Asp_{166} (**Min_1-A**) and the product complex in which the proton has been transferred from Asp_{166} to one of the oxygen atoms of the phosphorylated serine (**Min_2-A**) is only 0.9 kcal/mol. This small reaction energy for the deprotonation of Asp_{166} seems to be in accord with mutagenesis experiments in which replacement of Asp_{149} by an Asn in phosphorylase kinase (the analogue of Asp_{166} in PKA) leads to a fall of 4.5×10^3 in the rate of product release.[70] This experimental result and our calculations suggest a role for the negatively charged carboxylate group of Asp_{166} in promoting product release through intermediate structures similar to **Min_2-A**.

Another interesting aspect of the present simulations is the observed reaction coordinate distance between the nucleophilic oxygen atom and the phosphorus undergoing substitution. This distance has been estimated from the X-ray structures of PKA complexed with different substrate-analogues or inhibitors[19,28] and from NMR measurements,[63] giving a range of P···O distances between 2.7 and 5.3 Å.[68] Interestingly, a precise knowledge of the P···O distance is central to the development of bisubstrate protein kinase inhibitors, in which a mimic of the nucleophilic peptide is covalently linked to the γ-phosphorus of ATP at a distance matching the reaction coordinate distance. Previous attempts to develop bisubstrate inhibitors assumed a reaction coordinate distance of 1.7 Å,[72] compatible with a fully associative reaction mechanism, or a distance of 5.0 Å, assuming a fully dissociative mechanism.[65] Our QM study of the reaction mechanism shows that the energetically most favorable TS for the phosphoryl-transfer step has an 84% dissociative character, whereas the MD simulation of the ternary complex resulted in an average reaction coordinate distance of 3.8 ± 0.3 Å. These values could prove useful in the design of new PKA inhibitors.

In summary, the combined results from the MD simulation of the prereactive complex and the DFT optimizations of cluster

(70) Skamnaki, V. T.; Owen, D. J.; Noble, M. E. M.; Lowe, E. D.; Lowe, G.; Oikonomakos, N. G.; Johnson, L. N. *Biochemistry* **1999**, *38*, 14718−14730.
(71) Grant, B. D.; Adams, J. A. *Biochemistry* **1996**, *35*, 2022−2029.
(72) Medzihradszky, D.; Chen, S. L.; Kenyon, G. L.; Gibson, B. W. *J. Am. Chem. Soc.* **1994**, *116*, 9413−9419.

models of the cAMP-dependent protein kinase demonstrate that the carboxylate group of the invariant Asp_{166} participates in substrate binding, orients the hydroxyl group of the nucleophilic serine, and accepts its proton during the phosphoryl-transfer process through a dissociative mechanism. This theoretical picture of the reaction mechanism, in which Asp_{166} behaves as an acid/base catalyst, is in agreement with the main experimental observations concerning the phosphoryl-transfer process of protein kinases.

Acknowledgment. The authors thank the Commissariat à l′Energie Atomique and the Centre National de la Recherche Scientifique for support of this work. N.D. also acknowledges EMBO (Grant ALFT 371-2001) and the European Commission (Marie-Curie Fellowship Number IHP-HPMF-CT-2002-01759) for financial support. The optimized structures provided by Dr. Marat Valiev (UCSD) for comparative purposes are gratefully acknowledged. N.D. also acknowledges Dr. Dimas Suárez (University of Oviedo) for fruitful discussions.

Supporting Information Available: Proton affinities and geometries for an acetate anion, methyl phosphate dianion, and methyl phosphate dianion complexed with one and two Mg^{2+} ions. Geometries and relative enthalpies for a prereactive complex and a transition structure for the hydrolysis reaction of methyl phosphate dianion. Tables S1−S4 show the results of different analyses of the MD trajectory, whereas Table S5 displays the BCP properties of the charge density corresponding to the reactive P−O bonds (6 pages, print/PDF). This material is available free of charge via the Internet at http://pubs.acs.org.

JA037277U